

On the natural causes of global warming.

Abstract. Discussed in this review are the causes of global warming as well as its different aspects. It is demonstrated that temperature anomalies are inextricably linked to the speed of the magnetic North Pole, used as a proxy for the Earth's magnetic field; and UFO sightings, used as a proxy for energy transfer from the near-terrestrial space to the Earth's atmosphere. Also explained is why 2010 – 2016 was a very unusual period and how it affected global temperature and the environment.

Key words. Global warming, Earth's magnetic field, undetermined areal phenomena.

Introduction

1 In this review, we demonstrate a striking similarity between instrumentally measured tem-
 2 perature, the speed of the magnetic North Pole as a proxy for the Earth's magnetic field, seismic
 3 activity, and UFO sightings as a proxy for energy transfer between near-Earth space and the
 4 Earth's atmosphere. While many a pundit stridently clamor that UFOs are indicative of ex-
 5 traterrestrial aliens, we show that UFOs are but a facet in a large-scale natural phenomenon of
 6 solar-terrestrial origin. The similarity between global temperature and several other distinct and
 7 seemingly unrelated natural phenomena points towards the natural origin of global warming, which
 8 goes contrary to the current 97% consensus that global warming is caused by the greenhouse effect
 9 resulting from increased levels of CO_2 .

10 As a reference point for global temperature, we use Figure 1 exhibiting measurements by six
 11 reputable agencies. Figure 2 shows CO_2 concentration and emission, it bears no resemblance to
 12 and shows no correlation with Figure 1, other than that both CO_2 concentration and temperature
 13 in Figure 1 increased in 1980 – 2020. Yet, the remarkable similarity between temperature and the
 14 speed of the magnetic North Pole in 1900 – 2010 demonstrated in Figure 3 suggests that the Earth's
 15 magnetic field plays an important role in determining global temperature.

16 In pane I of Figure 3, the 1935 maximum in the speed of the magnetic North Pole appears
 17 to produce temperatures considerably higher than the larger 1950 maximum. The speed of the
 18 magnetic North Pole is but a simple facet of the Earth's magnetic field, it cannot be expected to
 19 reflect all aspects of the latter; that the temperatures corresponding to the 1935 maximum in the

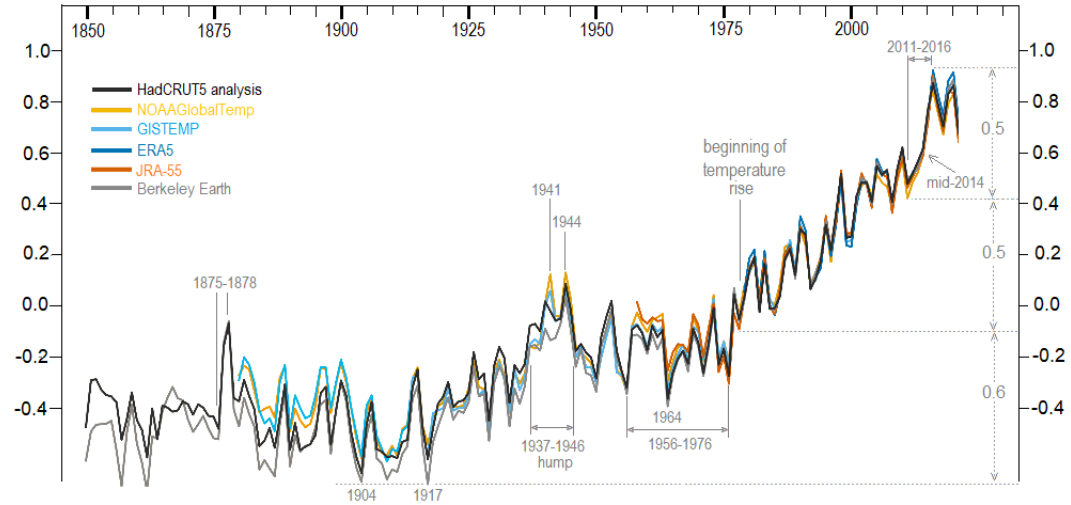


Figure 1: Annual global temperature anomalies in °C in 1900 – 2020 by six agencies, [1]. The largest known uninterrupted increase in global temperature occurred in 2011 – 2016.

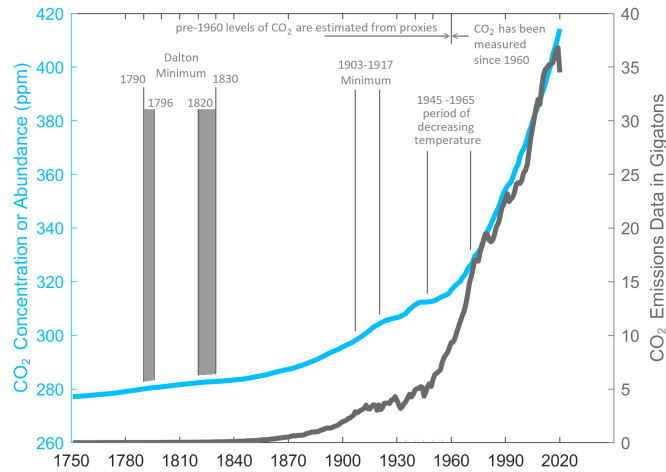


Figure 2: CO₂ concentration and emission. The original graph was produced and kindly emailed to the author of this paper by Dr. Howard Diamond, Climate Science Program Manager, NOAA. Comments were added by the author of this paper. The graph of CO₂ concentration bears no resemblance to and shows no correlation with the graphs in Figure 1, other than that CO₂ concentration and the graphs in Figures 1 increased in 1980 – 2020. Nor is the 1903 – 1917 temperature minimum reflected in the CO₂ graph in any way; as a matter of fact, the rate of increase of the CO₂ graph accelerated during the 1903 – 1917 temperature minimum. Even more bemusing is that the 1945 – 1965 period of decreasing temperature in Figure 1 seems to have coexisted with the rising levels of CO₂ shown above. The definition of the Dalton Minimum varies between 1790 – 1830 and 1796 – 1820, both options are shown; yet, whichever time window is chosen, the graph of CO₂ does not give even the tiniest hint of a temperature minimum.

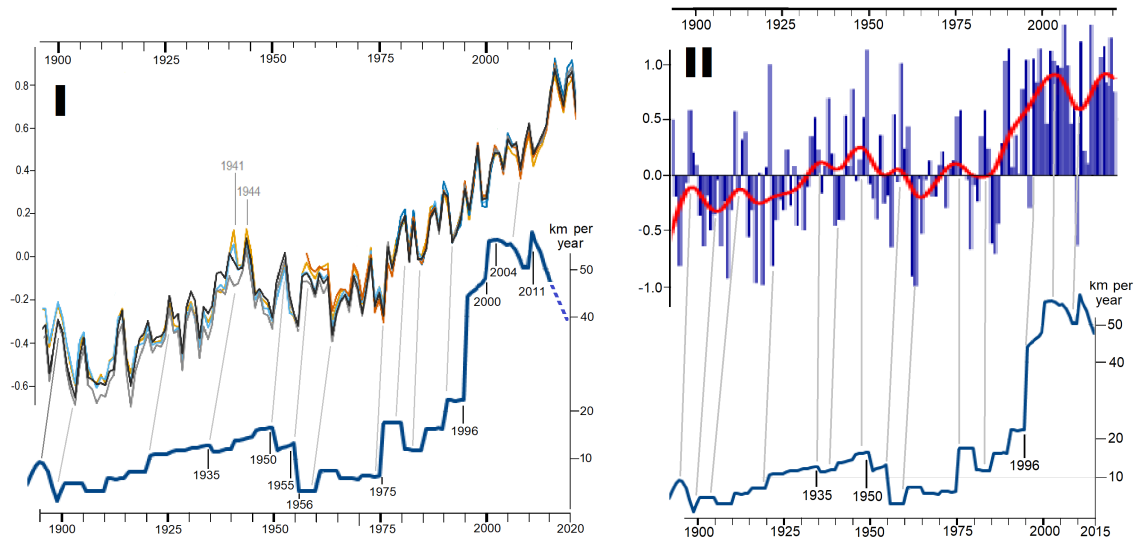
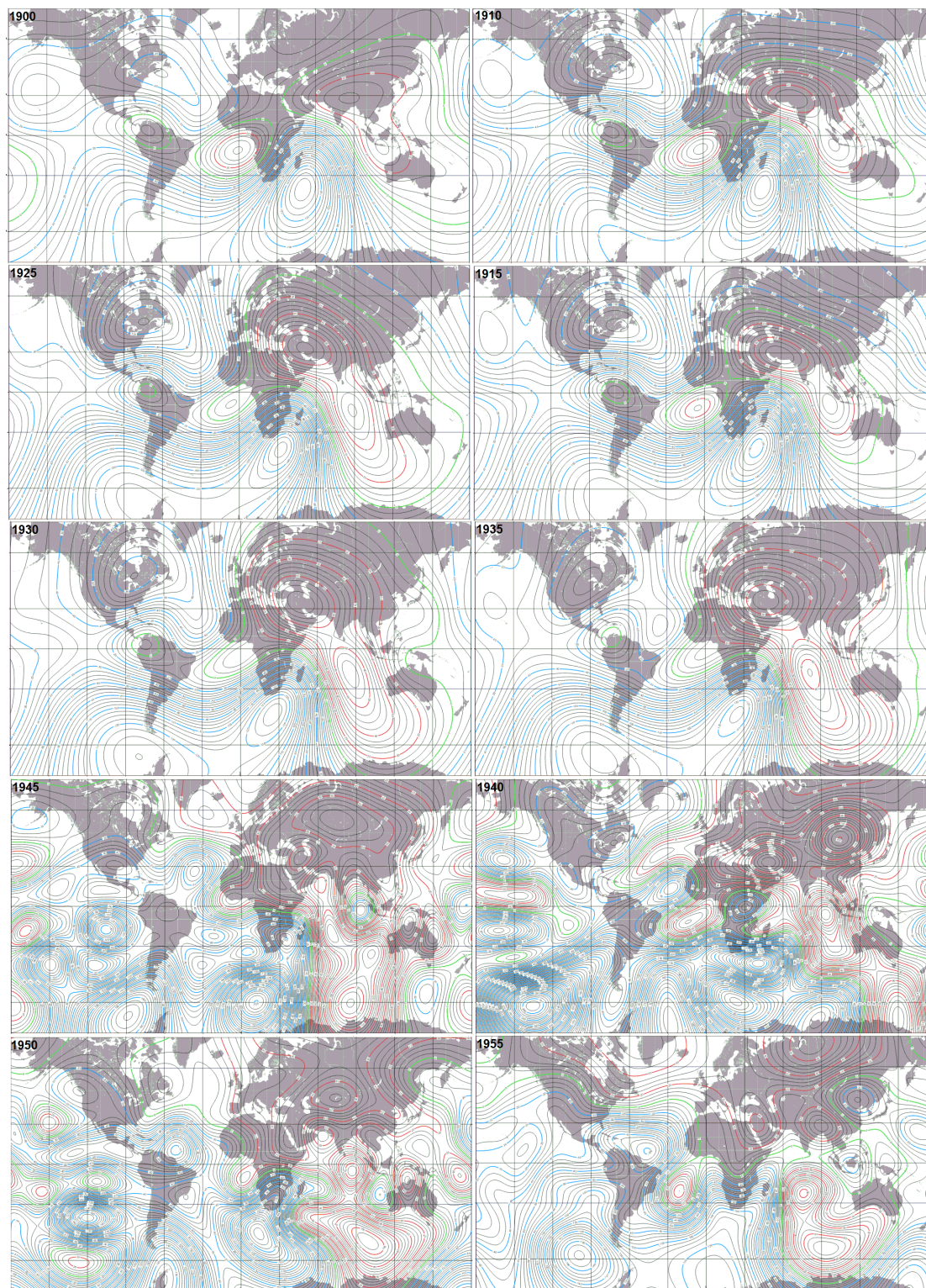
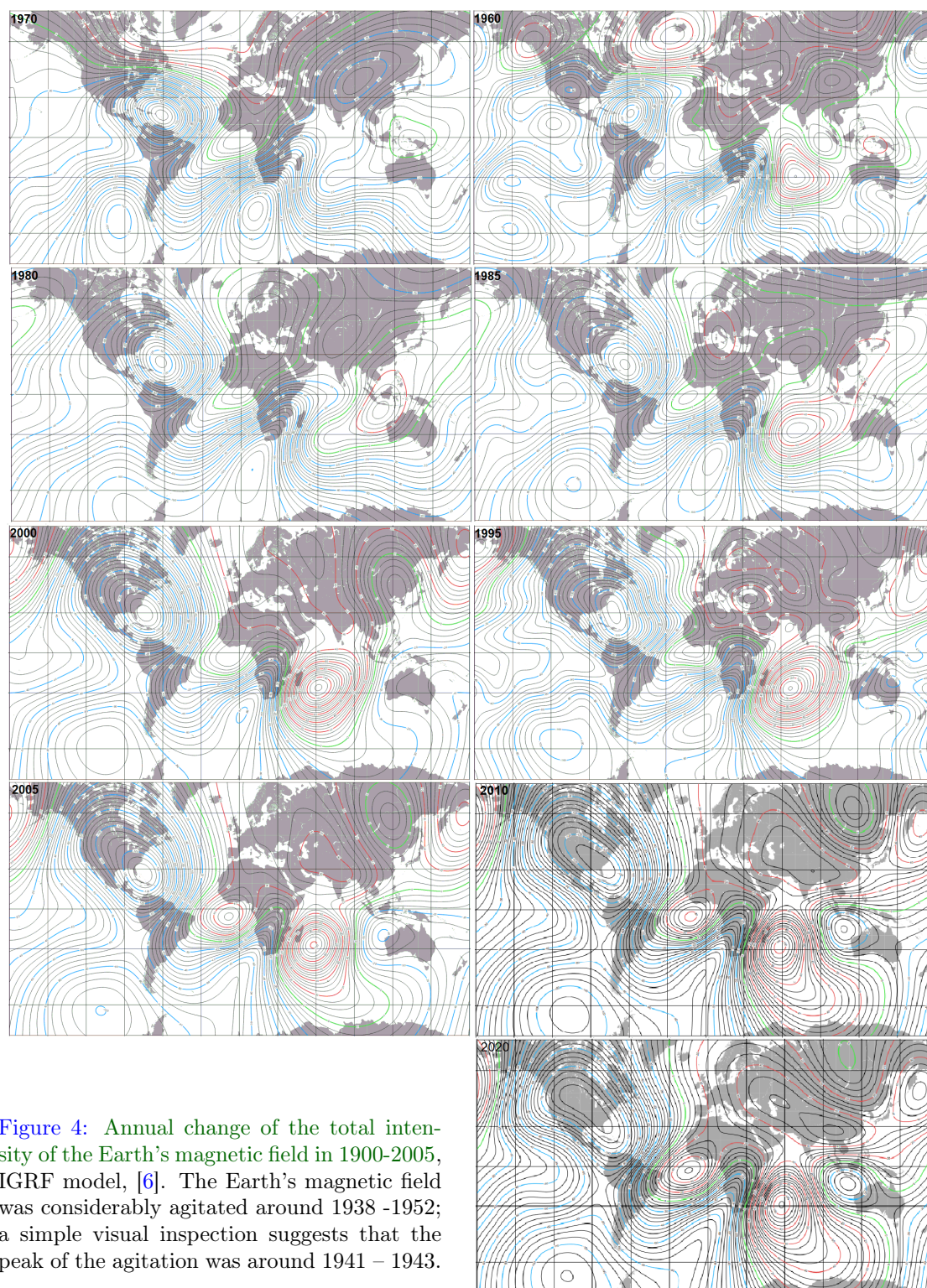


Figure 3: The top graph in pane I shows the 1900 – 2020 portion of Figure 1, the bottom graph shows the speed of the magnetic North Pole constructed from NOAA’s data, [3]; the 1900 – 2010 portions of the two graphs exhibit unequivocal similarity, the gray lines indicate which points on the two graphs correspond to each other. The top graph in pane II shows the mean Central England temperature annual anomalies in 1900 – 2010 in blue and its average in red, numerical data is from Met Office, [2], the bottom graph is the speed of the magnetic North Pole; the gray lines indicate which points on the two graphs correspond to each other. The Met’s temperature graph is very similar to the temperature record in Uppsala and Stockholm in Figure 1.1e in [4].

20 speed of the magnetic North Pole appear to be higher than those corresponding to the larger 1950
 21 maximum suggests geomagnetic activity at the time not reflected in the speed of the magnetic
 22 North Pole. Indeed, Figure 4 reveals a considerable agitation in the Earth’s magnetic field around
 23 1938 – 1952, accompanied by a power tussle described in Figure 5. These co-occurred with 1)
 24 the 1938 – 1946 increase in earthquake activity with 13 magnitude ≥ 8.0 earthquakes or 1.44
 25 earthquakes per year, for comparison, 1900 – 1999 saw 70 such earthquakes or 0.7 earthquakes per
 26 year, [5]; 2) an unusual increase in the number of unrecognized aerial phenomena, often referred
 27 to as *foo fighters*, unsuccessfully investigated by the Robertson Panel, *Projects Sign, Grudge, Blue*
 28 *Book*; and 3) 28 unusually powerful auroras on 1936/6/10, 1936/6/19, 1937/2/28, 1937/4/28,
 29 1937/8/3, 1938/1/25 Fatima geomagnetic storm, 1940/3/25, 1940/4/3, 1941/1/18, 1941/7/6,
 30 1941/9/18, 1942/6/27, 1943/9/4, 1944/10/15, 1944/12/17, 1946/2/3, 1946/3/24, 1946/4/8,
 31 1946/7/26, 1947/3/8, 1947/7/19, 1947/8/27, 1948/3/16, 1949/1/27, 1950/2/21, 1950/8/20,
 32 1951/7/2, 1951/9/23, [7]. A large number of powerful auroras suggests a considerable increase in
 33 solar activity; indeed, the solar activity must have been affected by the rare configuration of the





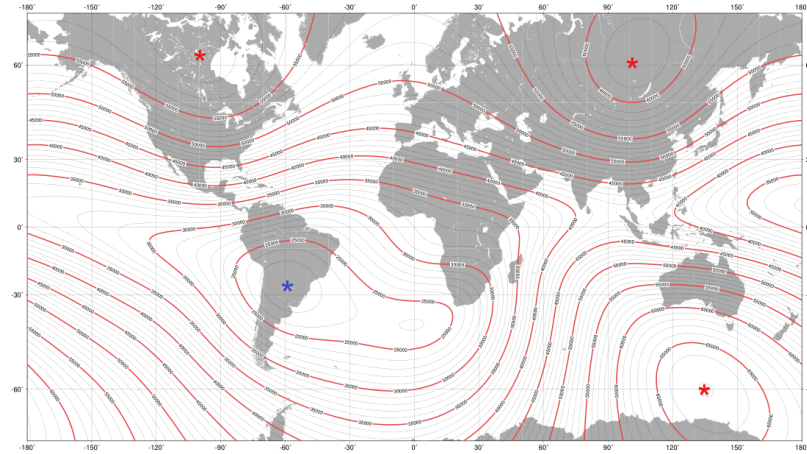


Figure 5: Total intensity of the Earth's magnetic field on 2020/1/1, [6]. The absolute minimum $22\,231.9\text{ nT}$ at $26.1^\circ\text{S}, 59.2^\circ\text{W}$ is marked by a blue asterisk. The three global maxima are marked by red asterisks: 1) North-Eastern maximum $61\,746.1\text{ nT}$ at $61.4^\circ\text{N}, 102.4^\circ\text{E}$, merely $\approx 59\text{ km}$ from the epicenter of the Tunguska explosion at $60.917^\circ\text{N}, 101.95^\circ\text{E}$; 2) North-Western maximum $58\,632.3\text{ nT}$ at $62.4^\circ\text{N}, 99.0^\circ\text{W}$, merely 56 km away from Angikuni Lake at $62.2^\circ\text{N}, 99.983333^\circ\text{W}$. 3) Southern maximum $66\,991.6\text{ nT}$ at $60.0^\circ\text{S}, 135.4^\circ\text{E}$. NOAA's model shows that the relative contribution of the North-Western maximum was larger than that of the North-Eastern maximum before 1948/11/27, while it was smaller after 1948/11/27, [6]. In reality, the tussle for superiority between the two maxima must have lasted for years with the baton changing hands more than once.

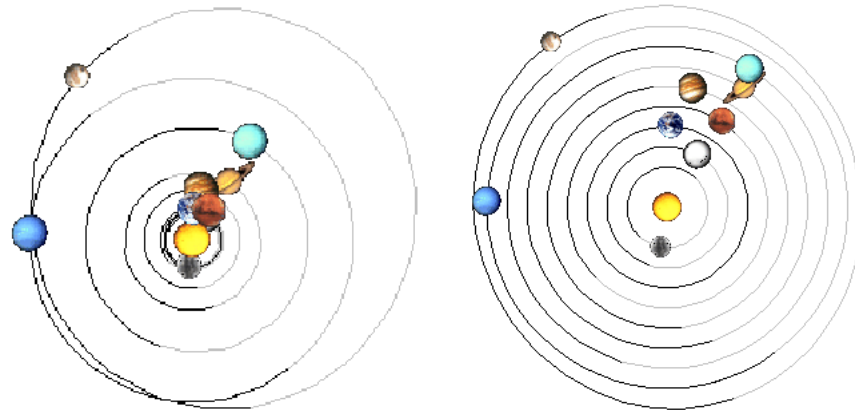


Figure 6: Solar system on 1941/12/18. On the left, orbits are shown in real configuration; on the right, orbits are shown as equidistant circles, [8]. With 1941/12/8 Jupiter opposition, 1941/11/17 Saturn opposition, 1941/11/21 Uranus opposition, 1941/11/10 Mars opposition, and 1942/2/2 Venus conjunction with Sun, 96.1% of the planetary mass of the Solar system almost lined up along a single line; of that Jupiter makes 71.2%, Saturn 21.3%, Uranus 3.3%, Earth 0.2%, and Venus 0.2%.

34 Solar System illustrated in Figure 6. The resulting increase in the solar activity must have been
 35 responsible for the auroras and, at least partially, contributed to the agitation of Figure 4 and
 36 additional temperature in 1938 – 1945 in pane I.

37 Let us now look at 2010 – 2016, when the influence of the Earth’s magnetic field on tem-
 38 perature was compounded by the tidal forces. On 2010/1/30, 2011/3/19, 2012/5/6, 2013/6/23,
 39 2014/8/10, 2015/9/28, and 2016/11/14, Full Moon and perigee came within, correspondingly, 165,
 40 59, 2, 23, 27, 65, and 150 minutes of each other synchronizing the increases in tidal pull due to
 41 Full Moon and perigee, [10]. Never in the known history have Full Moon and perigee been merely
 42 2 minutes apart as on 2012/5/6; nor have they been ≤ 65 minutes apart for 5 years in a row or
 43 ≤ 165 minutes apart for seven years in a row. The increases in tidal force due to the synchro-
 44 nization of Full Moon and perigee were further amplified by the 2010/1/29, 2012/5/7, 2013/6/20
 45 lunar nodes, and 2015/9/27 eclipse. We shall refer to a pair of a Full Moon and a perigee that
 46 come within 11 hours of each other as *Full Moon-perigee*, *New Moon-perigee* is defined similarly.
 47 Full Moon-perigees recur on average every 412 - 413 days, and so do New Moon-perigees. On
 48 2010/9/6, 2011/10/26, 2012/12/12, 2014/1/1, 2015/2/19, 2016/4/7 New Moon and perigee came
 49 within 9 hours of each other, which by itself is nothing to write home about, but the increase
 50 in tidal force was amplified by the 2010/9/4, 2011/10/29, 2012/12/11, 2015/2/21, 2016/4/5 lu-
 51 nar nodes, 2013/1/2, 2014/1/4 perihelia, 2010/9/21, 2011/10/29, 2012/12/3, 2014/1/5, 2015/2/6
 52 Jupiter oppositions, 2010/9/21 Uranus opposition, 2014/1/11 Venus-Sun conjunction, [9].

53 Although the increase in tidal force was rather small, it nevertheless brought the tidal force
 54 close to an all-time high, and must have contributed to unusual terrestrial events: 1) an unin-
 55 terrupted temperature rise in Figure 1; 2) a never-before-seen alignment of magnitude ≥ 7.9
 56 earthquakes with Full Moon-perigees shown in Table 1; 3) one of the only two known cases of three
 57 magnitude ≥ 8.5 earthquakes striking three years in a row on 2010/2/27, 2011/3/11, 2012/4/11,
 58 accompanied by the 2011/6/30-4 VEI=5 eruption of Puyehue, only once before three powerful
 59 earthquakes struck three years in a row on 1963/10/13, 1964/3/28, 1965/2/4, accompanied by the
 60 1963/3/18 VEI=5 eruption of Agung, [5, 13]; 4) the only observed space hurricane detected on
 61 2014/8/20, [15]. The synchronization of Full Moon and perigee may have also contributed to the
 62 only known appearance of the third Van Allen Belt on 2012/9/2, followed by waxing and waning
 63 of the Belts, obliteration of the outer and middle Belts, and final recovery of the known Belts’

64 structure, [14].

65 The mid-2014 – early 2015 was marked by never-before-seen undulations in cosmic ray in-
66 tensity shown in Figure 7 and the mid-2014 jump in the rate of temperature increase in Figure 1,
67 accompanied by the only observed space hurricane detected on 2014/8/20, [15]. Cosmic rays are
68 known to exhibit 27-day variability attributed to the solar synodic period; but never has the 27-day
69 variability been as clear and well-pronounced as in 2014/6/20 – 2015/2/13. Figure 7 points to the
70 Moon as a significant contributor to the undulations; since the only known source of energetic
71 particles that could be influenced by the Moon is the Van Allen Belts, we must conclude that the
72 undulations were produced by secondary particles created not only by cosmic rays but also by en-
73 ergetic particles from the Van Allen Belts. The tidal force produced by the synchronization of Full
74 Moon and perigee must have "shaken" the Van Allen Belts similarly to magnetopause shadowing,
75 when a solar emission, such as a gust of solar wind or a solar flare, temporarily changes the shape
76 of the Van Allen Belts interfering with the particles typical drift around magnetic lines and forcing
77 particles in all directions; the only difference is that the tidal force replaces solar emissions and is
78 applied periodically. A similar effect is produced by changes in the Earth's magnetic field, when
79 the changing shape of the magnetic lines interferes with particles' movement leading to the same
80 results as magnetopause shadowing.

81 What is somewhat problematic is that the energy of protons in the inner Van Allen Belt
82 is typically under 50 MeV, while the energy distribution of cosmic rays peaks around 300 MeV
83 with some particles's energy exceeding 10^{20} eV; that makes it rather difficult for protons from
84 the Van Allen Belts to disguise themselves as cosmic rays. recent work suggests that electrons
85 may be accelerated to ultra-relativistic energies, [19, 20, 21]. We may speculate that from mid-
86 2014 to early 2015, protons in the Van Allen Belts were also accelerated to cosmic ray energies
87 contributing to the undulations. The 2012 – 2015 period produced rather unusual events such as
88 the aforementioned space hurricane detected on 2014/8/20 and the third Van Allen Belt born on
89 2012/9/2, neither one has been completely explained; so it is not totally inconceivable that some
90 energetic particles in the Van Allen Belts could have been accelerated to the energies comparable
91 to those of cosmic rays. Of course, at other times, the Van Allen Belts still hurls energetic particles
92 at the atmosphere, albeit at lower speeds and with less energy.

93 If energetic particles from the Van Allen Belts contributed to the undulations, we may expect

Full Moon-perigees in 2010/1/1 – 2016/12/31	days between		Magnitude ≥ 7.9 earthquakes in 2010/1/1 – 2016/12/31	
2016/11/14	33	2016/12/17	M=7.9	Papua New Guinea
2015/9/28	12	2015/9/16	M=8.3	Alaska
2014/8/10	48	2014/6/23	M=7.9	Alaska
none		2014/4/1	M=8.2	Chile
2013/6/23	30	2013/5/24	M=8.3	Russia
none		2013/2/6	M=8.0	Solomon Islands
2012/5/6	25	2012/4/11	M=8.2	aftershock
2012/5/6	25	2012/4/11	M=8.6	Indonesia
2011/3/19	8	2011/3/11	M=7.9	aftershock
2011/3/19	8	2011/3/11	M=9.1	Japan
2010/1/30	28	2010/2/27	M=8.8	Chile

Table 1: Alignment of magnitude ≥ 7.9 earthquakes, [5], with Full Moon-perigees, [10]. Full Moon-perigees recur approximately every 412-413 days. In 2010/1/1 – 2017/1/1, $\approx 91\%$ of $M \geq 7.9$ earthquakes struck within 48 days of a Full Moon-perigee. If earthquakes struck randomly, only $\approx \frac{96}{412} \times 11 \leq 3$ earthquakes would be expected to strike within 48 days of a Full Moon-perigee; not all 9. The 2014/4/1 earthquake was not within 48 days of a Full Moon-perigee; however, it coincided with the 2014/3/30 – 2014/4/1 New Moon and lunar node and followed a rather unusual coalescence of the 2014/1/1 New Moon-perigee, 2014/1/4 perihelion, 2014/1/5 Jupiter opposition, 2014/1/11 Venus-Sun conjunction, and 2013/12/29 Mercury-Sun conjunction, all resulting in increased tidal force.

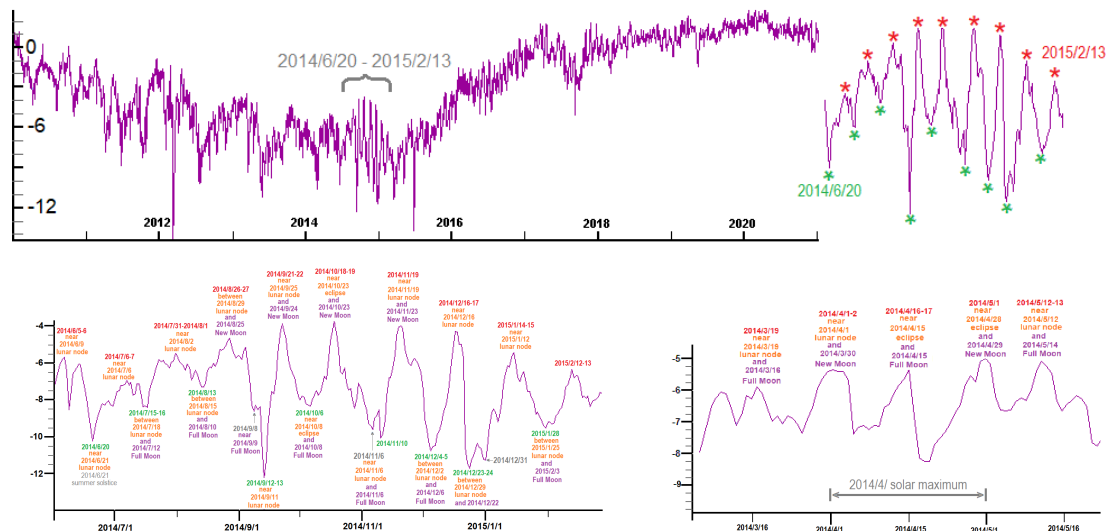


Figure 7: Cosmic rays variations, daily resolution, [11]. It shows rather unusual undulations in 2014/6/20–2015/2/13 with the maxima/minima marked correspondingly by red/green. Maxima/minima are close to lunar nodes, maxima are close to New Moon, minima are close to Full Moon, [10]. Although 27-day variability in cosmic rays is well-known, it has never been so strongly exhibited; nor is it well-understood for as [12] points out "existing theoretical models are not able to adequately reproduce characteristics of 27-day variations in the particle flux". The undulations were preceded by the 2014/3/15 – 2014/5/15 14-day recurrence of maxima shown in the bottom right pane, it has no analog in particle flux.

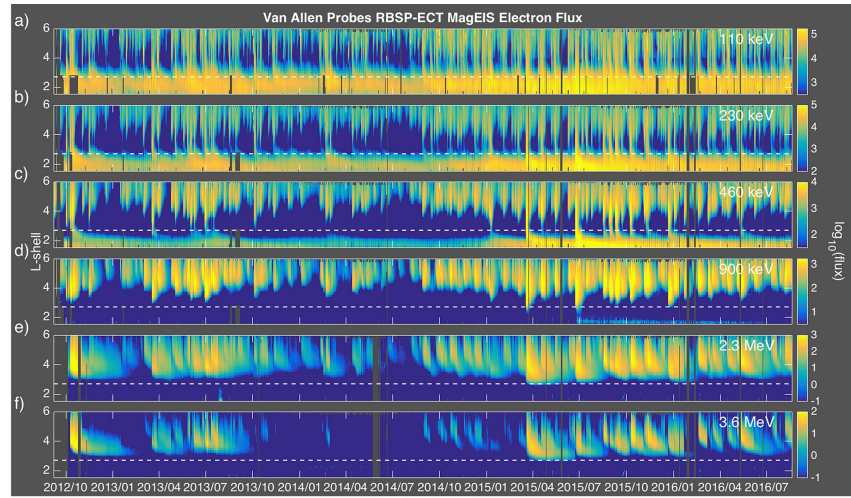


Figure 8: Electron differential fluxes in the inner Van Allen Belt from the MagEIS instruments on the Van Allen Probes spacecraft, [16]. Flux here is in units of $\#/(cm^2srKeV)$. Data from both RBSP A and B are shown in color ($\log_{10}(\text{flux})$) binned in time and L shell during the period from launch in September 2012 through February 2016. From top to bottom, each plot shows results from a different energy channel, as labeled in the top right of each plot. The graph shows flux drop for low L around 2013/10/ – 2015/3/.

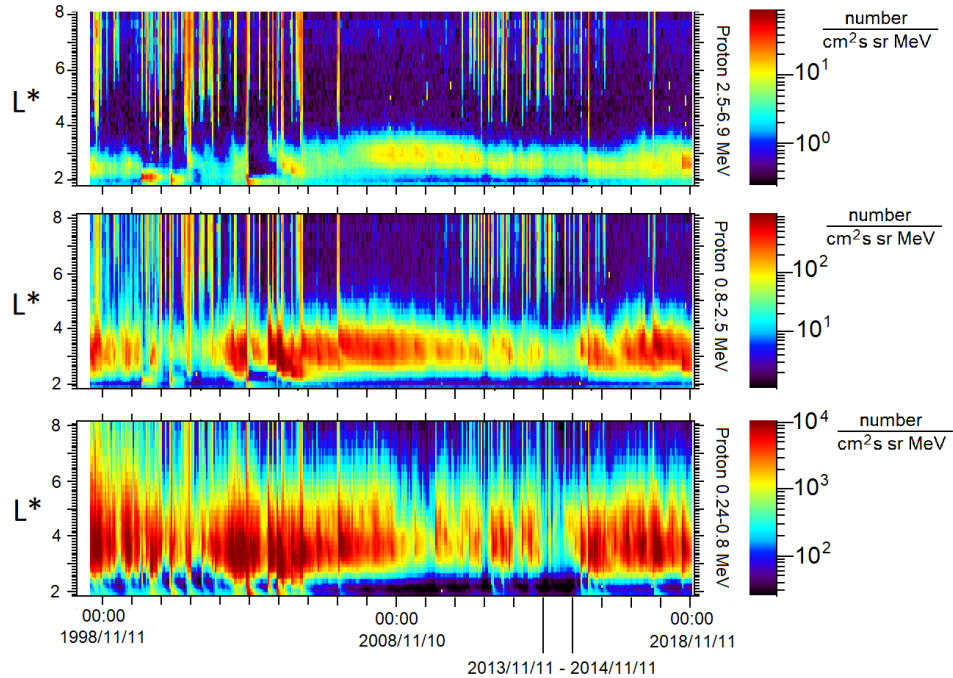


Figure 9: L-time cartographies of unidirectional proton flux measured by NPOES-15/SEM2 for several energies: 0.24-0.8 MeV (at the bottom), 0.8-2.5 MeV (in the middle) and 2.5-6.9 MeV (at the top), [17]. L^* is the radius (in Earth radii) of a particles drift around the Earth if the magnetic field adiabatically relaxed to a dipole configuration. The graph shows flux drop in the bottom and middle panes around 2013/11/ – 2014/11/.

94 the number of particles in the Van Allen Belts to drop around the time of the undulations. Indeed,
95 Figure 8 shows that the high-energy electron flux drastically dropped around the time of the
96 undulations, the mid-point of the drop falls on 2017/7/; Figure 9 shows that the proton flux also
97 decreased around 2013/11/ – 2014/11/, the mid-point falls on 2014/6/. Although 27-day variability
98 is easily seen in Figure 8, it is especially well-pronounced during 2014/8/ – 2015/5/ in the top
99 four rows. Recently considered 2014/8/25 – 2014/10/4 subperiod of the undulations was shown
100 to comprise three stages corresponding to intervals of increase/decrease in Figure 7: 1) 2014/8/27
101 – 2014/9/7, similar to HILDCAA; 2) 2014/9/13-20 with low flux of high energy electrons; and 3)
102 2014/9/22 – 2014/10/2, also similar to HILDCAA, [18].

103 Energetic particles entering Earth's atmosphere may produce lumps of highly-energetic sec-
104 ondary particles perceived by people as UFOs, which would explain almost daily encounters of
105 US Navy pilots with undetermined aerial objects high in the skies over the East Coast from the
106 summer of 2014 to March 2015 reported by the US Defense Department, [22]. Figure 10 shows
107 monthly and annual UFO sightings, they were considerably above average in 2011 – 2016, reaching
108 the all-time high at the time of the undulations in 2014/7/. As Figure 11 shows, the 1960 – 2010
109 portions of the graphs of UFO sightings and the speed of the magnetic North Pole are remarkably
110 similar; the graphs differ in 2010 – 2016 due to the synchronization of Full Moon and perigee.
111 Figure 13 shows a remarkable correlation between monthly UFO sightings and the bottom part of
112 Figure 9 around 2010 – 2016.

113 Since energetic particles in the Earth's atmosphere are expected to increase the latter's
114 temperature, we may expect a good correlation between the UFO sightings and temperature.
115 Indeed, Figure 14 shows a remarkable similarity between the graph of the annual global UFO
116 sightings in 1995/1/ – 1921/4/ and that of temperature anomalies in 1996/3/ – 2019/12/; the
117 similarity of the two graphs suggests that such energetic particles affect Earth's temperature and
118 are the main cause of current global warming. Even though pre-1995 UFO data contains too few
119 sightings, Figure 15 reveals some similarity between the graphs of the annual global UFO sightings
120 and temperature anomalies in 1960/1/1 – 1994/9/1; pre-1960 data is too sparse and potty to be
121 of any use. Unfortunately, the post-2018 UFO data is likely to be corrupted by Starlink satellites
122 reported by some as UFOs; so it is hard to make any future forecasts based on UFO sightings.
123 Figure 14 suggests that global temperature will go down for several years; what happens afterward

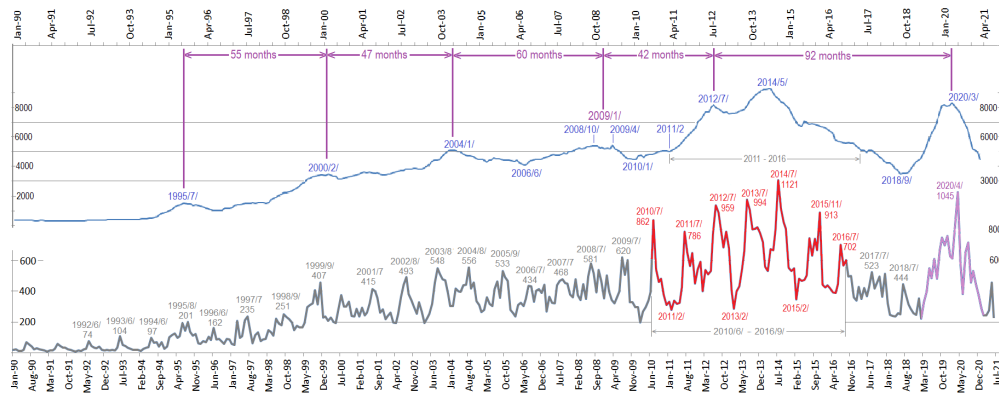


Figure 10: The bottom graph shows monthly global UFO sightings reported in 1990 – 2020, [23]. The top graph shows annual global sightings, the value at each month is calculated by adding the number of sightings in the month, in the preceding 6 months, and in the following 5 months. Pre-1995 counts are mostly in two digits and present too little information to be meaningful. Past-2018 data is likely to be corrupted by Starlink satellites.

124 depends on whether the 2020/3/ maximum in UFO sightings is a true maximum or a result of
 125 reports of Starlink satellites.

126 The correlation of global temperature in 1900 – 2017 with the speed of the magnetic North
 127 Pole and the magnetic South Pole’s rather sloth-like movement suggest that the largest temperature
 128 increase should be expected in the area around the two northern maxima of the total intensity of
 129 the Earth’s magnetic field defined in Figure 5 and/or the magnetic North Pole, Figure 16 shows
 130 that it is indeed so, and the highest temperature increases are between the two northern maxima
 131 of the total intensity of the Earth’s magnetic field; the very highest increase is right in front of
 132 the magnetic North Pole. While the parameters in Figure 16 were chosen by NASA to dramatize
 133 the effects of global warming, Figure 17 provides a somewhat more balanced view; it shows that
 134 the two northern maxima of the total intensity of the Earth’s magnetic field built two patches of
 135 increased temperature near them by 2009, in 2009 – 2012 a nexus developed between the patches
 136 along the path of the magnetic North Pole, by 2016 the nexus had widened to create a single large
 137 spot that extended to Europe by 2021. Figures 16, 17 illustrate how inextricably linked are the
 138 increasing temperature and the Earth’s magnetic field.

139 Mean Central England temperature annual anomalies is the longest record of instrument
 140 measurements of temperature going back to 1659. The speed of the magnetic North Pole in 1659
 141 – 1900 was too insignificant to affect temperature; in the absence of significant speed, curvature

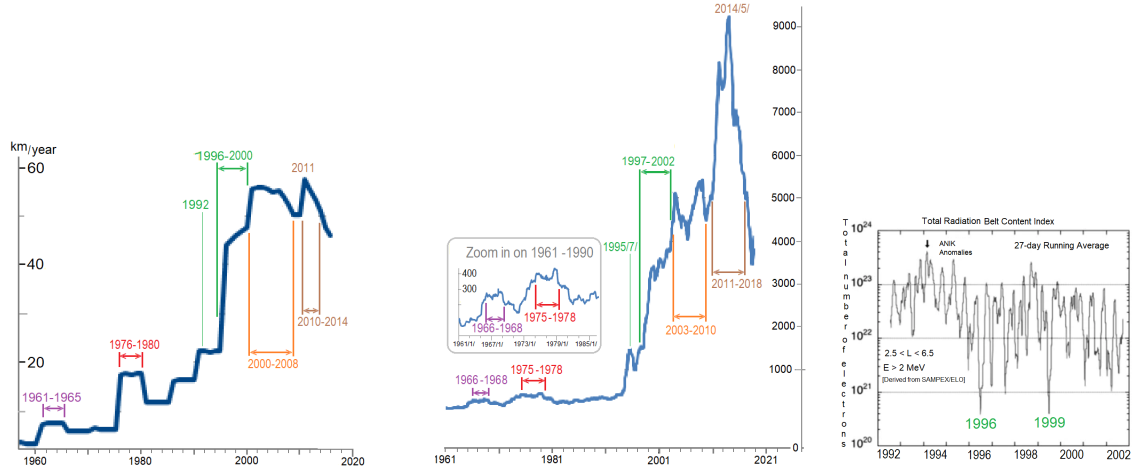


Figure 11: The graph on the left shows the speed of the magnetic North Pole based on the magnetic North Pole’s location on January 1 of the year, [3]; the graph in the middle shows the annual global UFO sightings for 1961 – 2020, [23], the inset zooms in on the 1961 – 1990 period. The graphs are not identical but exhibit very similar overall behavior, similar features are emphasized with similarly-colored labels. The speed of the magnetic North Pole does not appear to have counterparts of the 2004/1/ and 2009/1/ UFO peaks; however, Figure 12 shows that the graph of the magnetic North Pole’s speed does exhibit such counterparts if the resolution is even slightly improved. The graph on the right shows the total Radiation Belt Content index for the period 1992 – 2000 (monthly smoothing), [24]; two drastic drop-downs occurred in 1996 and 1999, right at the time of the two drastic increases in the magnetic North Pole’s speed.

Data for inset III			
Date	Coordinates of the magnetic North Pole	km moved in preceding 6 months	speed
1998/7/1	80.3N 108.067W		
1999/1/1	80.576N 108.597W	32	
1999/7/1	80.7N 109.13W	17	49
2000/1/1	80.972N 109.640W	32	49
2000/7/1	81.2N 110.30W	28	60
2001/1/1	81.427N 111.008W	28	56
2001/7/1	81.67N 111.78W	30	58
2002/1/1	81.879N 112.532W	26	56
2002/7/1	82.1N 113.35W	28	54
2003/1/1	82.325N 114.231W	28	56
2003/7/1	82.5N 114.96W	22	50
2004/1/1	82.762N 116.119W	33	55
2004/7/1	83.0N 117.24W	31	64
2005/1/1	83.186N 118.218W	24	55
2005/7/1	83.4N 119.38W	28	52
2006/1/1	83.602N 120.592W	27	55
2006/7/1	83.8N 121.88W	27	54
2007/1/1	83.995N 123.216W	27	54
2007/7/1	84.2N 124.78W	29	56
2008/1/1	84.363N 126.100W	23	52

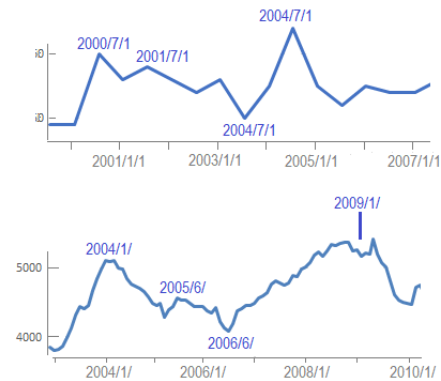


Figure 12: The table on the left shows the magnetic North Pole’s coordinates on January 1 and estimated coordinates on July 1 of the year, the speed is the distance covered in the preceding 12 months. So-defined speed is a slight improvement in resolution on the definition used in Figure 11. The top graph shows the speed of the magnetic North Pole, while the bottom graph zooms in on the 1961 – 1990 period of the UFO graph in Figure 11. The 2004/1/ and 2009/1/ peaks in UFO sightings correspond to the 2000/7/1 and 2004/7/1 peaks in the speed of the magnetic North Pole.

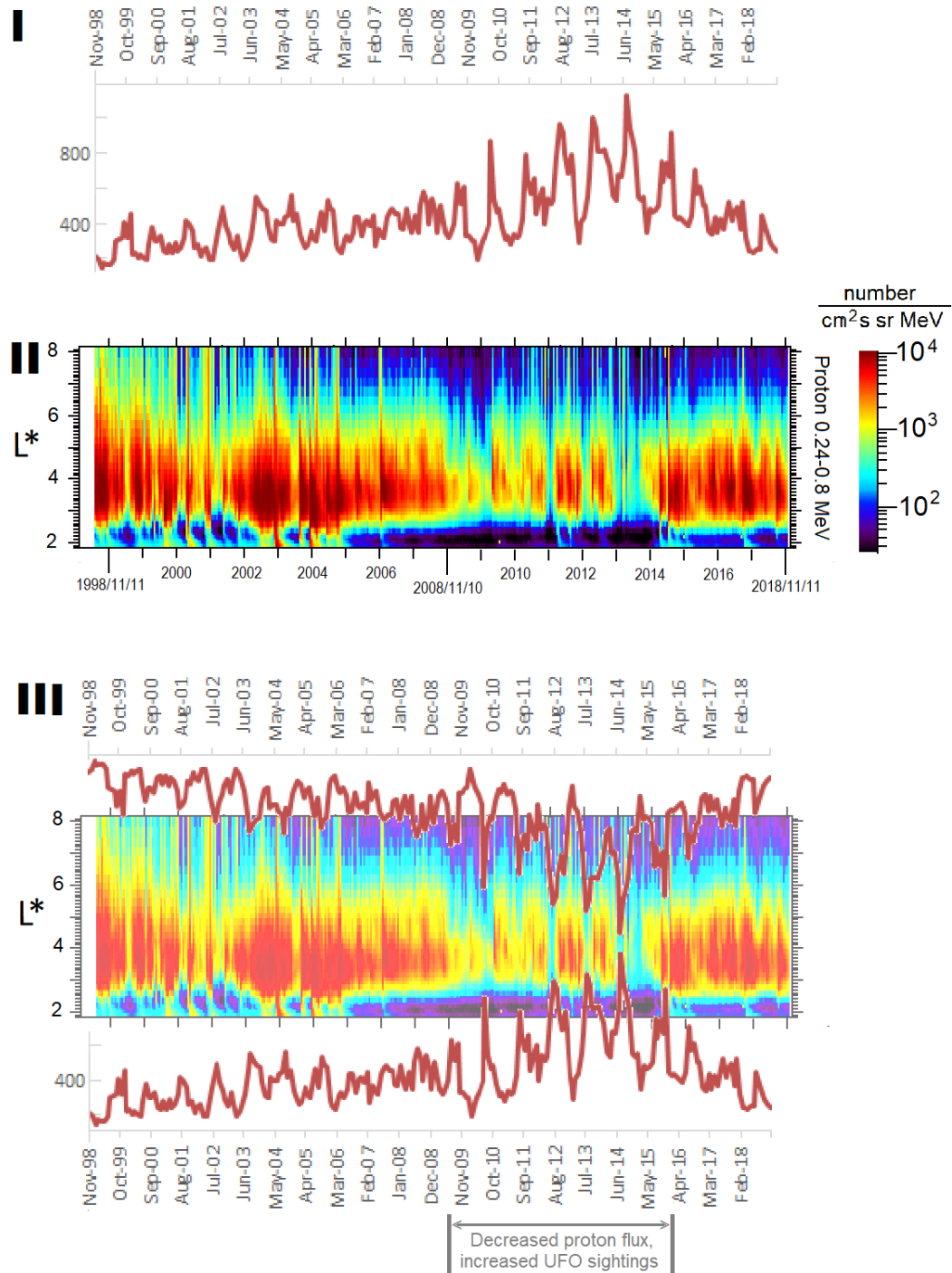


Figure 13: Frame I shows monthly UFO sightings from Figure 10, frame II shows the bottom part of Figure 9. In frame III, the graph from frame I and its inversion are superimposed on frame II with a ≈ 6.5 -month lag. UFO sightings mirror proton flux: the maxima in UFO sightings more-or-less coincide with the gaps between maxima in proton flux; that is especially well-pronounced in 2010 – 2016. The highest number of UFO sightings correspond to extremely low proton flux for $L < 2.5$.

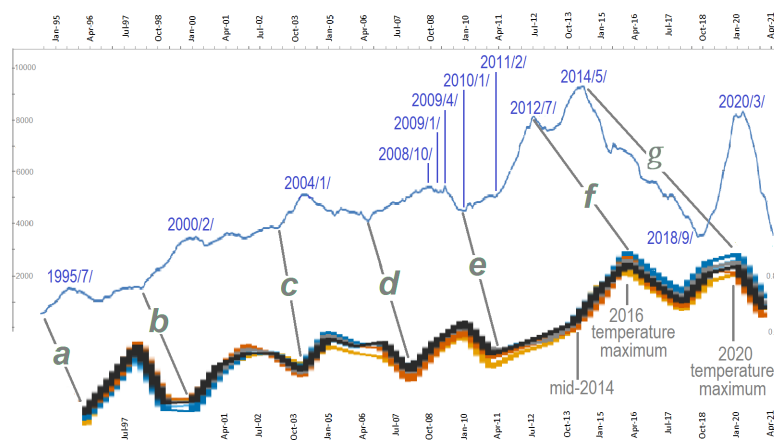


Figure 14: The top graph is the 1995/1/ – 1921/4/ annual global UFO sightings from Figure 10; the bottom graph is the 1996/3/ – 2019/12/ portion of Figure 1. The gray lines a - g divide both graphs into similar parts; the parts of the two graphs between each pair of consecutive gray lines are quite similar suggesting that the processes described by the two graphs are related. Lines e and f enclose both the largest uninterrupted temperature increase in the bottom graph and the largest uninterrupted increase in annual UFO sightings in the top graph. The 2014 and 2020 temperature maxima correspond to the 2012/7/ and 2014/5/ UFO maxima. The 2020 temperature maximum was only a few months after the first detection of Covid19.

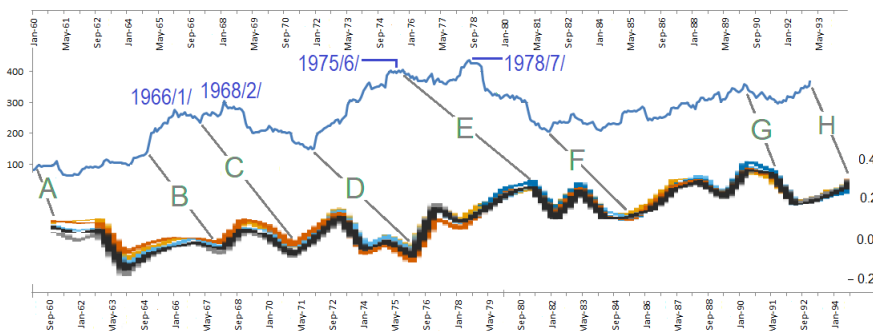


Figure 15: The top graph shows the annual global UFO sighting for 1960/1/ – 1993/1/ from Figure 10; the value for each month is calculated just like in Figure 14. The bottom graph is the 1960/9/ – 1994/9/ portion of Figure 1. Due to a rather small number of reported UFO sightings, the UFO graph does not properly reflect particle emissions from the Van Allen Belts, yet there is still some similarity between the graphs. The gray lines A - H divide both graphs into somewhat similar parts.

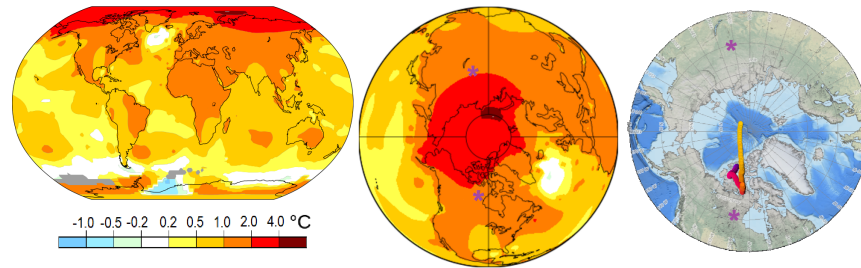


Figure 16: The left map shows NASA’s average surface air temperatures increase in 2011 – 2021 compared to the 1956-1976 average; it indicates that the largest temperature increases have occurred in the Northern hemisphere. The map was generated with a smoothing radius of 1200 km. The middle map was generated using NASA’s Scientific Visualization Studio generator with the same parameters as the top map, [25]. The modeled path of the magnetic North Pole in 1590 – 2022 is shown for reference only, [28]. The $\geq 2^{\circ}C$ temperature increase occurred around the two maxima of the total intensity of the Earth’s magnetic field defined in Figure 5; the $\geq 4^{\circ}C$ temperature increase occurred close to the current magnetic North Pole’s position. Purple asterisks mark approximate locations of the North-Eastern and North-Western maxima of the total intensity of the Earth’s magnetic field in 2020.

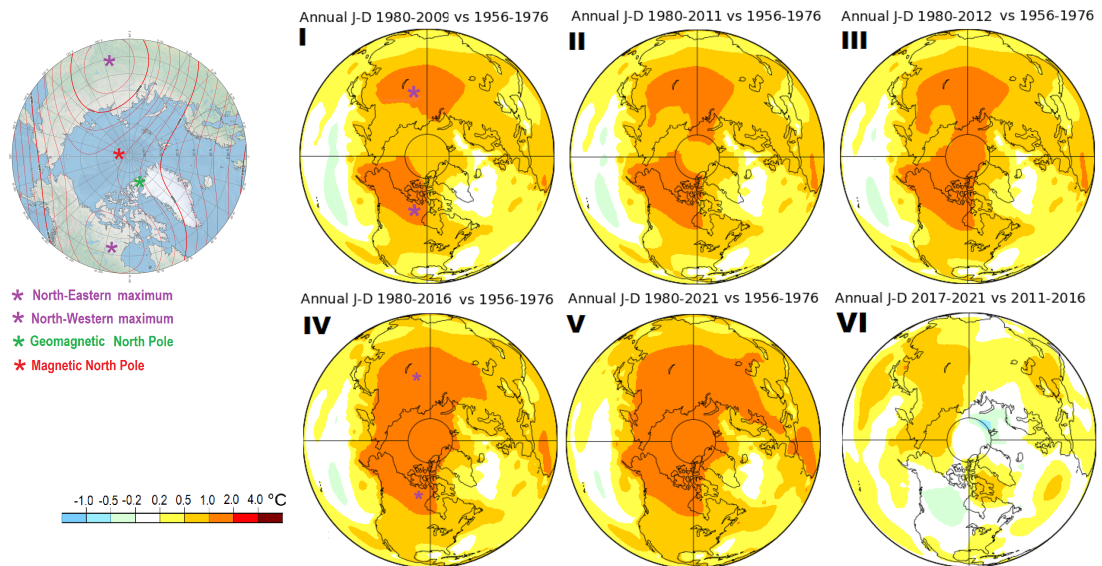


Figure 17: Evolution of the regions of $\geq 2^{\circ}C$ increase in the Northern hemisphere, generated using NASA’s Scientific Visualization Studio generator using the same parameters as in Figure 16, [25]. On the left is a map of the total intensity of the Earth’s magnetic field from WWM-2020 with the maxima of the total intensity of the Earth’s magnetic field in 2020 marked by purple asterisks, provided as a reference only. Frame I shows two patches of increased temperature that formed near the two northern maxima of the total intensity of the Earth’s magnetic field defined in Figure 5 by 2009; frames II and III shows the growth of a nexus connecting the two patches along the path of the magnetic North Pole in 2009 – 2012; frame IV shows how the nexus had widened by 2016 to create a single spot of increased temperature; frame V shows the moving of increased temperatures towards Europe. To avoid possible misinterpretation, frame VI is included to show that there was no drastic temperature increase in 2017 – 2021; the only left-over holdout of increasing temperature is around the North-Eastern maximum.

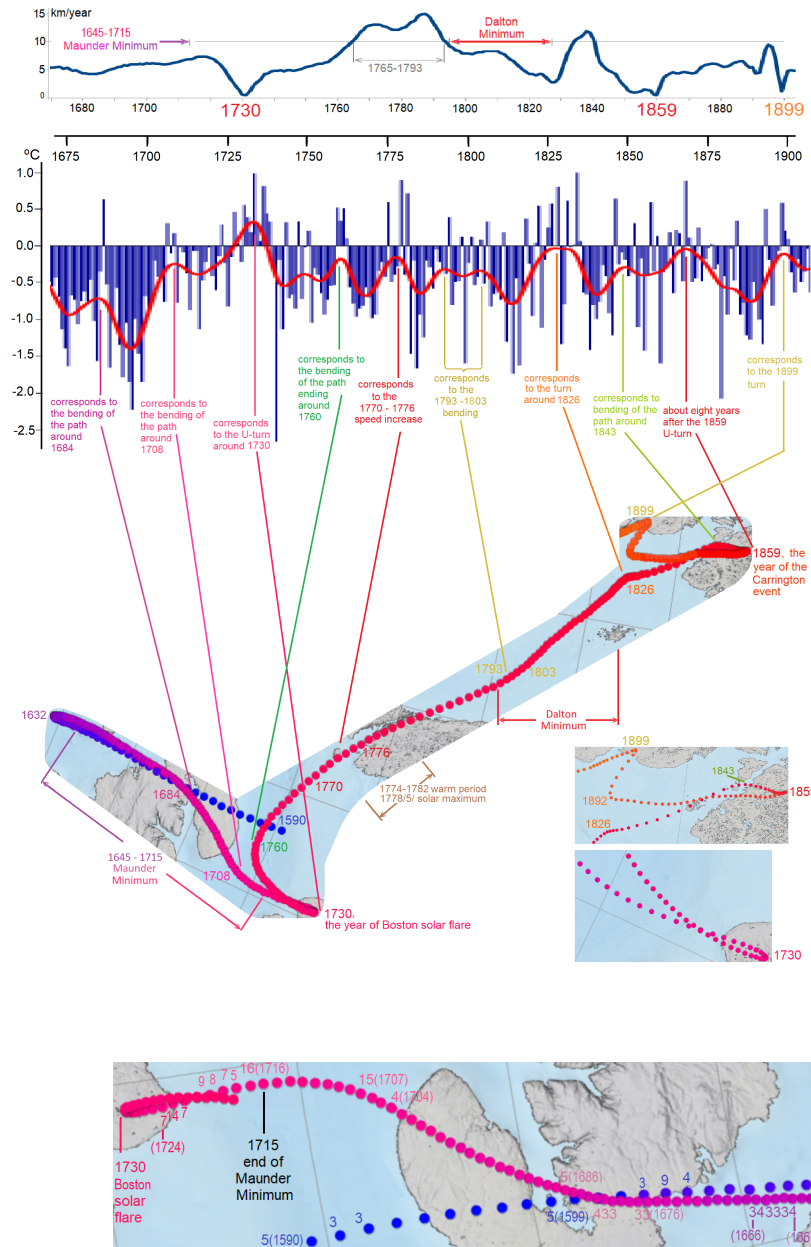


Figure 18: The top graph shows the speed of the magnetic North Pole. The middle graph shows the mean Central England temperature annual anomalies in 1659 – 2010 in blue, its average in red, [2]. The bottom graph shows the Magnetic North Pole’s path in 1590 – 1920, [28]; two insets zoom in on the crowded portions of the graph. Pre-1900 speed of the magnetic North Pole was insignificant; temperature depended more on the path’s curvature than the speed. The maxima of the red curve are matched with the turns of the path giving rise to them; although the matching is not perfect, it is sufficient to indicate the existence of a correlation between temperature and the movement of the magnetic North Pole. Colors are solely for visualization.

Figure 19: Auroras observed during the Maunder Minimum, [27], shown on the magnetic North Pole’s modeled path. The numbers of auroras for each year are shown only for years with ≥ 3 auroras. It shows a drastic increase in auroras contemporaneous with the 1632 U-turn in the path of the magnetic North Pole.

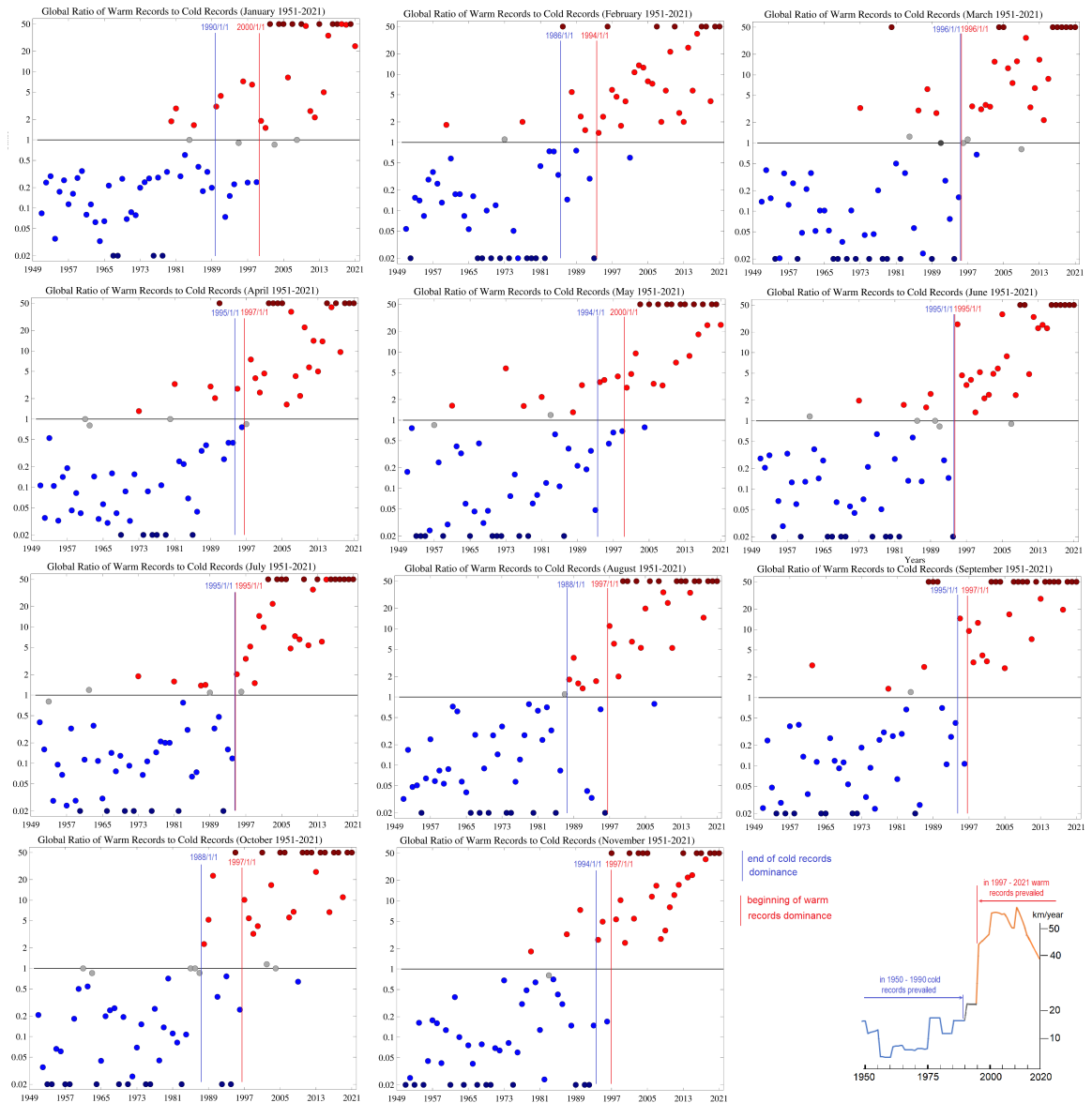


Figure 20: The ratio of warm-to-cold records for each month in 1951 – 2021, [29]; no data is available for December. A ratio value of X indicates that the global area experiencing record warm mean monthly temperatures over the most recent month was X times larger than the global area experiencing record cold conditions.

142 of the path of the magnetic North Pole seems to correlated with temperature, as Figure 18 shows.
 143 The Maunder and Dalton minima coincided with the portions of the magnetic North Pole’s path
 144 with low speed and low curvature, whereas higher temperature occurred when either the magnetic
 145 North Pole moved faster or its path showed considerable curvature.

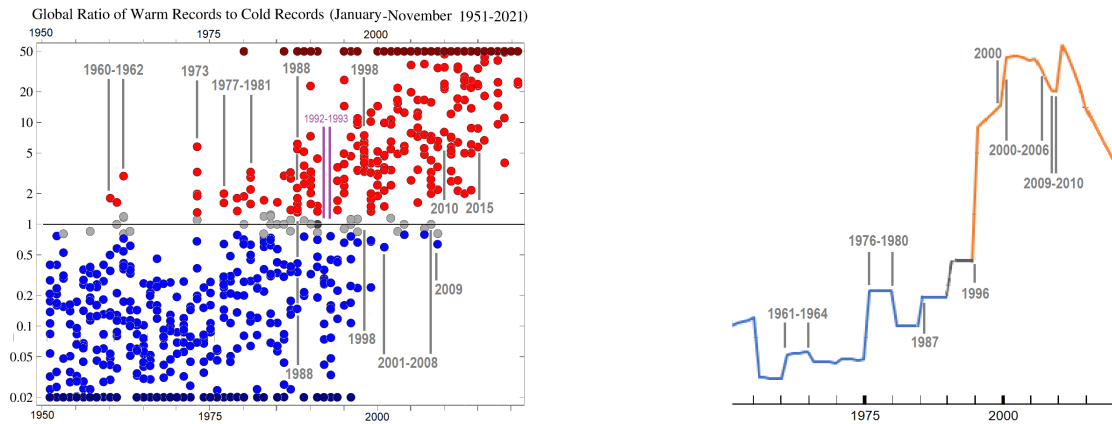


Figure 21: On the left, the 11 graphs of Figure 20 are superimposed together in one graph that shows a remarkable correlation with the speed of the magnetic North Pole on the right. The 1961 – 1964 slight increase in magnetic North Pole’s speed almost coincided with the first ≥ 1 ratios in 1960 – 1962; in 1976 – 1980 magnetic North Pole’s speed rose to 17 km/year causing more significant ≥ 1 ratios four years in a row in 1977 – 1981; the 1987 increase in the magnetic North Pole’s speed to 16 km/year led to the first year of ≥ 1 ratio prevalence in 1988; the VEI=6 eruption of Pinatubo and VEI=5 eruption of Hudson caused all ratios plunging to ≤ 1 in 1992 – 1993; the 1996 drastic increase in the magnetic North Pole’s speed to 44 km/year led to the prevalence of ≥ 1 ratios in 1997 and no ≤ 1 ratios in 1998; record high speed of the magnetic North Pole in 2000 – 2006 led to all ratios rising above 0.5 in 2001 and climbing above 0.2 in 2002 – 2008; the drop of the magnetic North Pole’s speed to 50 km/year in 2009 resulted in the smallest ratio since 2001 in 2009; the beginning of the Full Moon and perigee synchronization in 2010 led to all ratios rising to ≥ 2 in 2010 – 2021; the mid-2014 – early-2015 period led to all ratios rising to ≥ 4 in 2010 – 2021. The 1973 single-year increase in ≥ 1 ratio was most likely caused by an unusually large number of increases in tidal force: 1972/12/19-21 Full Moon, perigee, and lunar node; 1973/1/2-4 perihelion and eclipse; 1973/1/16-18 perigee and eclipse; 1973/5/4-6 lunar node, New Moon and perigee; 1973/6/1-2 New Moon-perigee and lunar node; 1973/6/16 eclipse; 1976/6/29-30 perigee and eclipse; 1973/7/17 eclipse; 1973/11/10-23 Full Moon, perigee, and lunar node; 1973/12/10 perigee and eclipse; 1973/12/24 eclipse.

146 Figure 20 shows NOAA’s graphs of cold and warm temperature records for January - Novem-
 147 ber. The graphs indicate that cold records prevailed from the first year of the graphs 1950 until
 148 1990 – 1992, that is when the speed of the magnetic North Pole was ≤ 17 km/year; while warm
 149 records have been prevailing since 1996 – 1997, when the speed of the magnetic North Pole was
 150 ≥ 20 km/year. The switch from cold records prevalence to warm records prevalence was accom-
 151 panied by a burst of nine magnitude ≥ 7.9 earthquakes on 1994/6/9, 1994/10/4, 1995/7/30,
 152 1995/10/9, 1995/12/3, 1996/1/1, 1996/2/17, 1996/6/10, 1996/6/17, [5], and two VEI ≥ 5 erup-
 153 tions on 1991/6/15, 1991/8/8; and was preceded by a slew of powerful solar flares: 1989/3/30
 154 X15.0, 1989/8/16 X20.0, 1989/9/29 X9.8, 1989/10/19 X13.0, 1990/5/24 X9.3, 1991/1/25 X10.0,

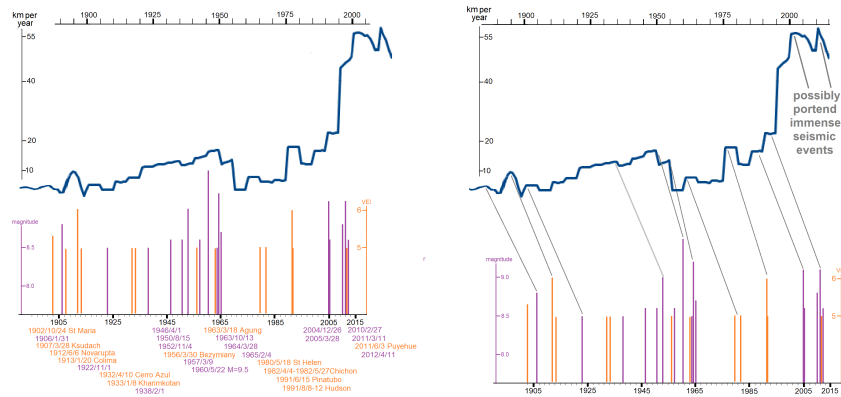


Figure 22: In the left pane, the speed of the magnetic North Pole is compared to the magnitude ≥ 8.5 earthquakes, shown in purple, and VEI ≥ 6 eruptions, shown in orange, in 1900 – 2015, [5, 13]. VEI=6 eruptions and magnitude ≥ 9.0 earthquakes are represented by lines of the same height as the frequencies of VEI=6 eruptions and magnitude ≥ 9.0 earthquakes are about the same; there were five VEI ≥ 5 eruptions and four magnitude ≥ 9.0 earthquakes in 1900 – 2021. The right frame shows the same graphs but with the time scales synchronized, gray lines connect powerful seismic events with the corresponding increases in the speed of the magnetic North Pole. The two graphs move in tandem in $\approx 1900 - 1996$, with seismic activity; each surge in the speed of the magnetic North Pole corresponds to a cluster of 1 - 3 seismic events ≈ 15 years later. The post-1996 high values of the magnetic North Pole's speed have no corresponding seismic events as if portending upcoming seismic events of immense proportions.

155 1991/6/1 X12.0, 1991/6/4 X12.0, 1991/6/6 X12.0, 1991/6/9 X10.0, 1991/6/11 X12.0, 1991/6/15
 156 X12.0, 1992/11/2 X9.0, [26]. It is hard to attribute the concomitance of 1) the change of the
 157 prevalence of cold records to the prevalence of warm records; 2) acceleration of the magnetic North
 158 Pole; 3) burst in seismic activity; 3) solar flare cannonade, to a mere coincidence. Given that 1)
 159 the 1632 U-turn was contemporaneous with drastically increased auroras as shown in Figure 19;
 160 2) the 1730 and 1859 U-turns were contemporaneous with the Boston solar flare on 1730/10/22
 161 and Carrington solar flare on 1859/9/1-2; 3) the Maunder and Dalton Minima coincided with the
 162 portions of the path with low speed and low curvature; 4) the 1950 increase in the speed of the
 163 Earth's magnetic field was amidst a host of solar flares and followed the alignment of planets in
 164 Figure 6 that was bound to increase solar emissions; we are justified to conclude that the drastic
 165 acceleration of the magnetic North Pole in 1996 – 2000 was most likely caused by solar emissions
 166 which included the aforementioned solar flare carronade. Since NOAA does not provide annual
 167 records, in Figure 21 all monthly records of Figure 20 are superimposed together, the obtained
 168 graph shows a remarkable correlation with the speed of the magnetic North Pole in 1951 – 2009.

Date & deaths		Airline, flight number, and a comment
NO SUCH ACCIDENTS IN 2017– 2021		
2016/5/19	66	EgyptAir 804, undetermined cause with evidence of fire onboard
2015/10/31	224	Metrojet 9268, undetermined cause, but blamed on terrorists
2015/3/24	150	Germanwings 9525, attributed to the co-pilot’s suicide
2014/12/27	162	AirAsia 8501, captain removed breaker to cut power
2014/7/24	116	Air Algerie 5017, obstruction of pressure sensors
2014/7/23	48	TransAsia Airways 222, unusual sounds before the crash, blamed on the crew
2014/3/7	227	Malaysia Airlines 370, just vanished
2013/11/29	33	LAM Mozambique Airline 470, attributed to the pilot’s suicide
2009/6/1	228	Air France 447, attributed to the crew’s mistakes
2005/10/25	117	Bellview Airlines 210, undetermined cause
2002/5/25	225	China Airlines 611, attributed to fatigue cracking
2000/1/10	10	Crossair 498, attributed to the pilot’s incapacitation
1999/10/31	217	EgyptAir 990, attributed to the pilot’s suicide
1998/9/2	229	Swissair 111, onboard fire of unknown origin
1997/12/19	104	SilkAir 185, attributed to the captain’s suicide
1996/7/17	230	TWA 800, an explosion of a fuel tank following a hit by a streak or flash of light of unknown origin
NO SUCH ACCIDENTS IN 1990 – 1995		

Table 2: Unexplained, or incompletely explained civilian airplane accidents in 1990 – 2021 much discussed in mass media, [31]. The six crashes in the 16 months of 2013/11/29 – 2015/3/24 averaged a crash every 3 months. Never before or after so many commercial airplanes crashed in such a short time. There were two accidents within 24 hours in July 2014, the unusual circumstances of one of them are discussed in Figure 23. Each accident may be googled for more information. Dates are linked to Aviation Safety Network, airlines with flight numbers are linked to Wikipedia articles.

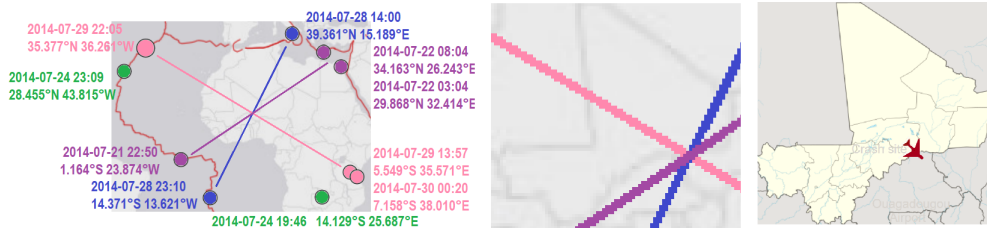


Figure 23: The right pane shows the crash site of Air Algerie 5017 on 2014/7/24, [32]. The left pane shows magnitude ≥ 4 earthquakes from 2014/7/21 22:00 UTC to 2014/7/30 1:00 UTC in $15^{\circ}S - 40^{\circ}N, 44^{\circ}W - 39^{\circ}E$, [5]. Quakes marked by the same color struck within 9.25 hours of each other, which we may consider being almost simultaneous. The line connecting one quake marked purple with the point between the other two, the line connecting the quakes marked pink, and the line connecting the quakes marked blue intersect at the same point, which is very close to the crash site of Air Algerie 5017. The straight lines, of course, represent great circles on the globe. The three lines look like a giant reticle pointing at the Air Algerie 5017 crash site. The middle pane zooms in on the intersection point to demonstrate how close it is to the crash site. This is an example of a rare phenomenon of the *seismic cross hairs*, its anatomy is to be discussed elsewhere.

169 Figure 22 reveals that even powerful seismic activity in 1900 – 2015 seems to have followed
170 the same pattern as global temperature and the speed of the magnetic North Pole.

171 With an increased number of aforementioned lumps of secondary energetic particles per-
172 ceived as UFOs, one may expect an increased number of airplane accidents. Indeed, 2013/11/29 –
173 2015/10/31 saw an unusually large number of commercial airplane accidents, those widely discussed
174 in media are shown in Table 2, 960 people died in merely 701 days of 2013/11/29 – 2015/10/31.
175 There was also a large number of close calls reported by crews of commercial airplanes, [30]. Eerie
176 circumstances of one of the accidents are illustrated in Figure 23. Those who find the connection
177 of airplane accidents to energetic particles far-fetched, should be reminded that the 1996/7/17
178 explosion of TWA 800 was preceded by a streak of light of unknown origin. The 1996 – 2002
179 airplane crashes were contemporaneous with the 1996 – 2000 increase in the speed of the magnetic
180 North Pole and 1996 – 2002 increase in the annual UFO sightings.

181 Figure 1 shows low temperature during 1907 – 1911, likely due to a diminished contribution
182 of energetic particles from the Van Allen Belts. We may speculate that, for whatever reason, the
183 energetic particles at the time did not enter the Earth's atmosphere in the usual way but instead
184 as a large lump causing the Tunguska explosion. The proximity of the Tunguska explosion to the
185 North-Eastern maximum of the total intensity of the Earth's magnetic field speaks in favor of the
186 hypothesis.

187 §1 Concluding remarks.

188 The current global warming has been attributed to increased levels of CO_2 ; yet, the graphs
189 of temperature and CO_2 bear no resemblance. In 1900 – 2010 global temperature practically
190 mirrored the behavior of the speed of the magnetic North Pole, powerful seismic activity, while the
191 areas most affected by global warming were near the two northern maxima of the total intensity
192 of the Earth's magnetic field and the magnetic North Pole. In 2010 – 2016, global temperature
193 and UFO sightings were also influenced by tidal forces in addition to the Earth's magnetic field.
194 The demonstrated correlation between global temperature, movement of the magnetic North Pole,
195 and UFO sightings cannot be explained by increased levels of CO_2 but can be explained by our
196 hypothesis.

197 Truly bewildering is the currently popular view that different geophysical phenomena such

198 as earthquakes and eruptions, movement of the magnetic poles, auroras, etc. are unrelated to each
199 other; hardly can be attributed to a mere coincidence the concomitance of 1) an unusually high
200 frequency of unexplained or incompletely-explained airplane accidents in 2013/11/29 – 2015/10/31
201 illustrated by Table 2; 2) almost daily encounters of US Navy pilots with undetermined aerial
202 objects from the summer of 2014 to March 2015, [22]; 3) the all-time high of UFO sightings in the
203 middle of 2014 in Figure 10; 4) unusual and never-before-seen undulations of Figure 7; 5) the only
204 known case of a space hurricane detected on 2014/8/20, [15]; 6) depletion of the Van Allen Belts
205 around 2014 illustrated by Figures 8, 9; 7) a sudden jump in the derivative of global temperature
206 in mid-2014 exhibited in Figure 1. Already in 1923 in his book *New Lands*, Charles Fort suggested
207 that so-called UFOs were coming from near-terrestrial space; while in the 1950s, Dr J. Allen Hynek
208 suggested that the so-called UFOs are likely to be a natural phenomenon. It is quite likely that
209 some, if not all, airplane accidents of Table 2 were caused by lumps of highly-energetic secondary
210 particles perceived by people as UFOs; had proper research been done, the disasters might have
211 been mitigated.

212 References

- 213 [1] Global temperature, [https://public.wmo.int/en/media/press-release/state-of-](https://public.wmo.int/en/media/press-release/state-of-climate-2021-extreme-events-and-major-impacts)
214 [climate-2021-extreme-events-and-major-impacts](https://public.wmo.int/en/media/press-release/state-of-climate-2021-extreme-events-and-major-impacts), [https://climate.metoffice.](https://climate.metoffice.cloud/temperature.html)
215 [cloud/temperature.html](https://climate.metoffice.cloud/temperature.html). An interactive graph is available at [https://ourworldindata.](https://ourworldindata.org/co2-and-other-greenhouse-gas-emissions)
216 [org/co2-and-other-greenhouse-gas-emissions](https://ourworldindata.org/co2-and-other-greenhouse-gas-emissions).
- 217 [2] Mean Central England Temperature, <https://www.metoffice.gov.uk/hadobs/hadcet/>,
218 https://www.metoffice.gov.uk/hadobs/hadcet/cet_info_mean.html, based on Parker
219 et al (1992), [https://www.metoffice.gov.uk/hadobs/hadcet/Parker_etaliJOC1992_](https://www.metoffice.gov.uk/hadobs/hadcet/Parker_etaliJOC1992_dailyCET.pdf)
220 [dailyCET.pdf](https://www.metoffice.gov.uk/hadobs/hadcet/Parker_etaliJOC1992_dailyCET.pdf). Numerical dataset [https://www.metoffice.gov.uk/hadobs/hadcet/](https://www.metoffice.gov.uk/hadobs/hadcet/cetml1659on.dat)
221 [cetml1659on.dat](https://www.metoffice.gov.uk/hadobs/hadcet/cetml1659on.dat).
- 222 [3] Williams, B., The Correlation of North Magnetic Dip Pole Motion and Seismic Activity,
223 *Journal of Geology and Geophysics*, 2016, [https://www.longdom.org/open-access/the-](https://www.longdom.org/open-access/the-correlation-of-north-magnetic-dip-pole-motion-and-seismic-activity-2381-)
224 [correlation-of-north-magnetic-dip-pole-motion-and-seismic-activity-2381-](https://www.longdom.org/open-access/the-correlation-of-north-magnetic-dip-pole-motion-and-seismic-activity-2381-)

- 225 8719-1000262.pdf, data from <https://www.ngdc.noaa.gov/geomag/data/poles/NP.xy>.
- 226 The graph was kindly emailed to the author of the paper on 2021/1/1.
- 227 [4] Johann Hiebl, The early instrumental climate period (1760-1860) in Europe, evidences from
228 the Alpine region and Southern Scandinavia, thesis, [https://www.meteologos.rs/wp-](https://www.meteologos.rs/wp-content/uploads/2019/12/THE-EARLY-INSTRUMENTAL-CLIMATE-PERIOD-IN-EUROPE_1760-1860.pdf)
229 [content/uploads/2019/12/THE-EARLY-INSTRUMENTAL-CLIMATE-PERIOD-IN-EUROPE_](https://www.meteologos.rs/wp-content/uploads/2019/12/THE-EARLY-INSTRUMENTAL-CLIMATE-PERIOD-IN-EUROPE_1760-1860.pdf)
230 [1760-1860.pdf](https://www.meteologos.rs/wp-content/uploads/2019/12/THE-EARLY-INSTRUMENTAL-CLIMATE-PERIOD-IN-EUROPE_1760-1860.pdf)
- 231 [5] USGS earthquake catalog <https://earthquake.usgs.gov/earthquakes/search/> and
232 NOAA earthquake database [https://www.ngdc.noaa.gov/hazel/view/hazards/](https://www.ngdc.noaa.gov/hazel/view/hazards/earthquake/search)
233 [earthquake/search](https://www.ngdc.noaa.gov/hazel/view/hazards/earthquake/search).
- 234 [6] NOAA: maps <https://www.ngdc.noaa.gov/geomag/magfield-wist/>, database [https://](https://www.ngdc.noaa.gov/geomag/calculators/magcalc.shtml#igrfgrid)
235 www.ngdc.noaa.gov/geomag/calculators/magcalc.shtml#igrfgrid.
- 236 [7] Space Weather Archives, <http://www.solarstorms.org/SRefStorms.html>.
- 237 [8] NASA's Solar System calculator, <https://www.fourmilab.ch/cgi-bin/Solar>.
- 238 [9] Jupiter syzygies. For 2002 – 2021 http://iaaras.ru/media/data/ae2021/ae_d4e.txt
239 with the year appropriately selected; for 1991 – 2021 [https://www.planetary.org/](https://www.planetary.org/articles/06031044-oppositions-conjunctions-rpx)
240 [articles/06031044-oppositions-conjunctions-rpx](https://www.planetary.org/articles/06031044-oppositions-conjunctions-rpx); for 1990 – 2021 *Astronomical Phe-*
241 *nomena for the Year 2021* with 2021 replaced by the required year; for 1912 – 1989
242 *Observer's handbook 1989* at [https://www.rasc.ca/sites/default/files/publications/](https://www.rasc.ca/sites/default/files/publications/ObserverHandbook-1989.pdf)
243 [ObserverHandbook-1989.pdf](https://www.rasc.ca/sites/default/files/publications/ObserverHandbook-1989.pdf) with 1989 replaced by the required year from. Non-scientific
244 <http://www.astrology.com.pl/transits/2021/> with 2021 replaced by the appropriate year
245 might be the most convenient to use.
- 246 [10] Lunar events <http://astropixels.com/ephemeris/moon/moonnodes2001.html> and [https://](https://www.fourmilab.ch/earthview/pacalc.html)
247 www.fourmilab.ch/earthview/pacalc.html
- 248 [11] Moscow Neutron Monitor <http://cr0.izmiran.ru/mosc/main.htm>, Oulu Neutron Moni-
249 tor <https://cosmicrays oulu.fi/>. Other monitors and data <https://www.nmdb.eu/nest/>,
250 <http://neutronm.bartol.udel.edu/>.

- 251 [12] Yulbarisov, R.F., Galikyan, N.G., Mayorov, A.G. et al. Amplitude and Temporal Char-
252 acteristics of 27-Day Variations in the Galactic Cosmic Ray Flux, Measured during the
253 PAMELA Experiment between 2006 and 2016. *Bull. Russ. Acad. Sci. Phys.* 85, 12721275
254 (2021). <https://doi.org/10.3103/S1062873821110381>.
- 255 [13] Eruptions databases, [https://www.ngdc.noaa.gov/hazel/view/hazards/volcano/event-](https://www.ngdc.noaa.gov/hazel/view/hazards/volcano/event-search)
256 [search](https://volcano.si.edu/search_eruption.cfm), https://volcano.si.edu/search_eruption.cfm.
- 257 [14] Van Allen Belts in 2012, <https://www.science.org/doi/10.1126/science.1233518>,
258 [https://www.scientificamerican.com/article/third-van-allen-radiation-belt-](https://www.scientificamerican.com/article/third-van-allen-radiation-belt-makes-appearance-around-earth/)
259 [makes-appearance-around-earth/](https://www.scientificamerican.com/article/third-van-allen-radiation-belt-makes-appearance-around-earth/)
- 260 [15] Qing-He Zhang et al, A space hurricane over the Earth's polar ionosphere, *Nature Communi-*
261 *cations*, vol. 12, article number: 1207 (2021), [https://www.nature.com/articles/s41467-](https://www.nature.com/articles/s41467-021-21459-y)
262 [021-21459-y](https://www.nature.com/articles/s41467-021-21459-y).
- 263 [16] D. L. Turner, T. P. O'Brien, J. F. Fennell, S. G. Claudepierre, J. B. Blake, A. N. Jaynes,
264 D. N. Baker, S. Kanekal, M. Gkioulidou, M. G. Henderson, G. D. Reeves, Investigating
265 the source of near-relativistic and relativistic electrons in Earth's inner radiation belt, *GJR*
266 *Space Physics*, vol. 122, issue1, 2017, pp. 695-710, [https://agupubs.onlinelibrary.wiley.](https://agupubs.onlinelibrary.wiley.com/doi/full/10.1002/2016JA023600)
267 [com/doi/full/10.1002/2016JA023600](https://agupubs.onlinelibrary.wiley.com/doi/full/10.1002/2016JA023600). Similar graphs at [https://angeo.copernicus.](https://angeo.copernicus.org/preprints/angeo-2018-98/angeo-2018-98.pdf)
268 [org/preprints/angeo-2018-98/angeo-2018-98.pdf](https://angeo.copernicus.org/preprints/angeo-2018-98/angeo-2018-98.pdf), [https://agupubs.onlinelibrary.](https://agupubs.onlinelibrary.wiley.com/doi/full/10.1029/2018JA025277)
269 [wiley.com/doi/full/10.1029/2018JA025277](https://agupubs.onlinelibrary.wiley.com/doi/full/10.1029/2018JA025277).
- 270 [17] Sicard, A., Bourdarie, S., Lazaro, D., Standarovski, D., Ecoffet, R., et al. A new model for
271 the 1-10 MeV proton fluxes (part of ONERA GREEN-V3 model). European Conference on
272 Radiation and its Effects on Components and Systems (RADECS) 2019, Montpellier, France.
273 <https://hal.archives-ouvertes.fr/hal-02797017/document>
- 274 [18] Jaynes, A. N., et al. (2015), Source and seed populations for relativistic electrons: Their
275 roles in radiation belt changes, *J. Geophys. Res. Space Physics*, 120, pp. 7240-7254, [https:](https://agupubs.onlinelibrary.wiley.com/doi/10.1002/2015JA021234)
276 [//agupubs.onlinelibrary.wiley.com/doi/10.1002/2015JA021234](https://agupubs.onlinelibrary.wiley.com/doi/10.1002/2015JA021234). The portion quoted is
277 under Figure 4.

- 278 [19] Allison, H., Shprits, Yu., Local heating of radiation belt electrons to ultra-relativistic energies,
279 *Nature Communications*, 2020; 11: 4533, [https://www.ncbi.nlm.nih.gov/pmc/articles/
280 PMC7483540/](https://www.ncbi.nlm.nih.gov/pmc/articles/PMC7483540/).
- 281 [20] Allison, H., Shprits, Yu., Zhelavskaya, I., Wang, D., Smirnov, A., Gyroresonant wave-particle
282 interactions with chorus waves during extreme depletions of plasma density in the Van Allen
283 radiation belts, *Science Advances*, 2021, Vol 7, Issue 5, [https://www.science.org/doi/10.
284 1126/sciadv.abc0380](https://www.science.org/doi/10.1126/sciadv.abc0380).
- 285 [21] Zhang, X., Artemyev, A., Angelopoulos, V. et al. Superfast precipitation of energetic electrons
286 in the radiation belts of the Earth. *Nat Commun* 13, 1611 (2022). [https://www.nature.com/
287 articles/s41467-022-29291-8#citeas](https://www.nature.com/articles/s41467-022-29291-8#citeas)
- 288 [22] *New York Times* [https://www.nytimes.com/2019/05/26/us/politics/ufo-sightings-
289 navy-pilots.html](https://www.nytimes.com/2019/05/26/us/politics/ufo-sightings-navy-pilots.html)
- 290 [23] UFO Reporting Center, <http://www.nuforc.org/webreports/ndxevent.html>.
- 291 [24] Baker, D.N., Erickson, P.J., Fennell, J.F. et al. Space Weather Effects in the Earths Radiation
292 Belts. *Space Sci Rev* 214, 17 (2018), Figure 29. [https://link.springer.com/article/10.
293 1007/s11214-017-0452-7](https://link.springer.com/article/10.1007/s11214-017-0452-7)
- 294 [25] NASA's Scientific Visualization Studio generator is at [https://data.giss.nasa.gov/
295 gistemp/maps/index_v4.html](https://data.giss.nasa.gov/gistemp/maps/index_v4.html); the parameters are taken from [https://en.wikipedia.org/
296 wiki/Instrumental_temperature_record](https://en.wikipedia.org/wiki/Instrumental_temperature_record), [https://commons.wikimedia.org/wiki/File:
297 Change_in_Average_Temperature.svg](https://commons.wikimedia.org/wiki/File:Change_in_Average_Temperature.svg).
- 298 [26] Most powerful solar flares known, [https://www.spaceweatherlive.com/en/solar-
299 activity/top-50-solar-flares.html](https://www.spaceweatherlive.com/en/solar-activity/top-50-solar-flares.html), http://www.ioffe.ru/LEA/Solar/1994_en.html,
300 <https://www.spaceweather.com/solarflares/topflares.html>, [https://www.sws.bom.
301 gov.au/Educational/2/3/9](https://www.sws.bom.gov.au/Educational/2/3/9).
- 302 [27] Schroeder, W., On the Existence of the 11-Year Cycle in Solar and Auroral Activity before
303 and during the so-called Maunder Minimum, *Journal of geomagnetism and geoelectricity*, 1992
304 vol. 44 issue 2 pp.119-128, [https://www.jstage.jst.go.jp/article/jgg1949/44/2/44_2_
305 119/_article](https://www.jstage.jst.go.jp/article/jgg1949/44/2/44_2_119/_article).

- 306 [28] NOAA, Modelled magnetic poles' paths, [https://www.ncei.noaa.gov/maps/historical_](https://www.ncei.noaa.gov/maps/historical_declination/)
307 [declination/](https://www.ncei.noaa.gov/maps/historical_declination/). Proper boxes need to be checked.
- 308 [29] NOAA, Global area at record levels for 1951 – 2021. To access a specific month use link
309 <https://www.ncdc.noaa.gov/sotc/global/2021XX/supplemental/page-3> with XX re-
310 placed by 01 for January, 02 for February, ..., 11 for November; there is no data for December.
311 For example, July may be accessed at [https://www.ncdc.noaa.gov/sotc/global/202107/](https://www.ncdc.noaa.gov/sotc/global/202107/supplemental/page-3)
312 [supplemental/page-3](https://www.ncdc.noaa.gov/sotc/global/202107/supplemental/page-3), it is also available at [https://commons.wikimedia.org/wiki/File:](https://commons.wikimedia.org/wiki/File:202107_Percent_of_global_area_at_temperature_records_-_Global_warming_-_NOAA.svg)
313 [202107_Percent_of_global_area_at_temperature_records_-_Global_warming_-](https://commons.wikimedia.org/wiki/File:202107_Percent_of_global_area_at_temperature_records_-_Global_warming_-_NOAA.svg)
314 [_NOAA.svg](https://commons.wikimedia.org/wiki/File:202107_Percent_of_global_area_at_temperature_records_-_Global_warming_-_NOAA.svg).
- 315 [30] Nine confirmed close-call encounters with UFOs, a) [https://www.thestar.com/news/](https://www.thestar.com/news/canada/2016/11/14/porter-plane-in-near-miss-with-drone.html)
316 [canada/2016/11/14/porter-plane-in-near-miss-with-drone.html](https://www.thestar.com/news/canada/2016/11/14/porter-plane-in-near-miss-with-drone.html); b) [https://www.theguardian.com/technology/2016/apr/28/heathrow-ba-plane-strike-not-](https://www.theguardian.com/technology/2016/apr/28/heathrow-ba-plane-strike-not-a-drone-incident)
317 [a-drone-incident](https://www.theguardian.com/technology/2016/apr/28/heathrow-ba-plane-strike-not-a-drone-incident), c) [http://www.denverpost.com/business/ci_27872975/denver-](http://www.denverpost.com/business/ci_27872975/denver-bound-icelandair-flight-from-reykjavik-hit-by)
318 [bound-icelandair-flight-from-reykjavik-hit-by](http://www.denverpost.com/business/ci_27872975/denver-bound-icelandair-flight-from-reykjavik-hit-by); d) [http://www.dailymail.co.](http://www.dailymail.co.uk/news/article-3034472/Hero-Loganair-pilot-pulls-plane-North-Sea-nosedive-just-SEVEN-SECONDS-spares.html?ITO=1490&ns_mchannel=rss&ns_campaign=1490)
319 [uk/news/article-3034472/Hero-Loganair-pilot-pulls-plane-North-Sea-nosedive-](http://www.dailymail.co.uk/news/article-3034472/Hero-Loganair-pilot-pulls-plane-North-Sea-nosedive-just-SEVEN-SECONDS-spares.html?ITO=1490&ns_mchannel=rss&ns_campaign=1490)
320 [just-SEVEN-SECONDS-spares.html?ITO=1490&ns_mchannel=rss&ns_campaign=1490](http://www.dailymail.co.uk/news/article-3034472/Hero-Loganair-pilot-pulls-plane-North-Sea-nosedive-just-SEVEN-SECONDS-spares.html?ITO=1490&ns_mchannel=rss&ns_campaign=1490); e)
321 <http://avherald.com/h?article=47d74074>; f) 8 [http://www.atsb.gov.au/media/](http://www.atsb.gov.au/media/4897226/AO-2014-052%20Final.pdf)
322 [4897226/AO-2014-052%20Final.pdf](http://www.atsb.gov.au/media/4897226/AO-2014-052%20Final.pdf); g) [http://www.huffingtonpost.com/2014/01/06/](http://www.huffingtonpost.com/2014/01/06/ufo-jet-airliner-near-miss-over-uk_n_4549399.html)
323 [ufo-jet-airliner-near-miss-over-uk_n_4549399.html](http://www.huffingtonpost.com/2014/01/06/ufo-jet-airliner-near-miss-over-uk_n_4549399.html); h) [http://www.dailymail.](http://www.dailymail.co.uk/news/article-2339139/Was-bird-A-Plane-Or-UFO--Chinese-passenger-jet-hits-mysterious-object-26-000ft-lands-severely-dented-nose-cone.html)
324 [co.uk/news/article-2339139/Was-bird-A-Plane-Or-UFO--Chinese-passenger-jet-](http://www.dailymail.co.uk/news/article-2339139/Was-bird-A-Plane-Or-UFO--Chinese-passenger-jet-hits-mysterious-object-26-000ft-lands-severely-dented-nose-cone.html)
325 [hits-mysterious-object-26-000ft-lands-severely-dented-nose-cone.html](http://www.dailymail.co.uk/news/article-2339139/Was-bird-A-Plane-Or-UFO--Chinese-passenger-jet-hits-mysterious-object-26-000ft-lands-severely-dented-nose-cone.html), [http:](http://cayodagyo.blogspot.com/2013/06/some-possibilities-of-object-that-had.html)
326 [//cayodagyo.blogspot.com/2013/06/some-possibilities-of-object-that-had.html](http://cayodagyo.blogspot.com/2013/06/some-possibilities-of-object-that-had.html);
327 <http://cayodagyo.blogspot.com/2013/06/some-possibilities-of-object-that-had.html>;
328 i) <http://www.ibtimes.co.uk/ufo-plane-glasgow-scotland-463308#>.
- 329 [31] Unexplained, or not completely explained civilian airplane accidents in 2013 – 2016
330 much discussed in mass media. Aviation Safety Network <https://aviation-safety.net/>
331 and Wikipedia. Crashes at takeoff or landing, crashes of Boeing 747 Max, crashes
332 of military planes like [https://en.wikipedia.org/wiki/2016_Indian_Air_Force_An-32_](https://en.wikipedia.org/wiki/2016_Indian_Air_Force_An-32_disappearance)
333 [disappearance](https://en.wikipedia.org/wiki/2016_Indian_Air_Force_An-32_disappearance), and crashes of small aircraft like <https://www.cbc.ca/news/canada/>

- 334 [calgary/tsb-report-jim-prentice-plane-crash-release-1.4635541](#) are not included in
335 the table.
- 336 [32] Air Algeirie 5017, https://en.wikipedia.org/wiki/Air_Al%C3%A9rie_Flight_5017